SSRG International Journal of Geo-informatics and Geological Science
ISSN: 2393–9206 / https://doi.org/10.14445/23939206/IJGGS-V13I2P103
Volume 13 Issue 2, 24-38, May-Aug 2026


*Original Article*

# Comparative Analysis of Hydraulic Flood Models in Mapping Flood Vulnerable Areas in Abia State, Nigeria

Baywood, C. N[1], Igbokwe, J.I.[2]

[1]*Department of Surveying and Geo-Informatics, Federal University of Technology, Owerri.*
[2]*Department of Surveying and Geoinformatics, Nnamdi Azikiwe University, Awka.*

[1]*Corresponding Author : igbokweesom@gmail.com*

Received: 02 June 2026 Revised: 07 July 2026 Accepted: 24 July 2026 Published: 08 August 2026

***Abstract*** *- Studying issues and risks associated with flooding is a thing of utmost importance, especially for a developing country like Nigeria. Flooding, being an event that occurs regularly with so many predictions of its constant hazardous effect, there is a pressing need to analyze and understudy the available methodology and ascertain the most suitable, with proven results for modelling flood risk vulnerability. Therefore, this paper, as part of research, is aimed at the analysis and assessment of the accuracy of hydraulic flood models in mapping flood vulnerability areas in Abia State, Nigeria. Its objectives were to: examine the pattern of landcover/landuse; determine the surface runoff potential; model the extent of flood vulnerability using HEC-RAS, TUFLOW, and Flood Modeler; and compare and analyze the results obtained. The methodology involved the acquisition of Sentinel-2 imagery covering Abia State, Rainfall data and ALOS PALSAR. Image subsetting was done to extract the area of study from the acquired dataset. This was followed by analysis of DEM accuracy using root mean square error, image classification to extract the landuse/landcover of the study area, surface runoff modelling to determine surface runoff potential in the study area and hydraulic flood modelling using HecRAS, TUFLOW AND flood modeler. The results indicated that ALOS PALSAR was a fit to be used for flood modeling, as backed by the vertical and horizontal accuracies of 5.64m and 14.39m, respectively. The flood frequency return as modelled by HecRAS revealed a 25.43km$^2$ inundation extent in a 2-year return period, 28.09km$^2$ inundation extent for a 5-year period and 26.67km$^2$ inundation extent for a 10-year return period, increasing to its peak extent by 3.15% by the 5-year return period, then decreasing by 1.8% by the 10-year return period. The flood frequency return as modelled by TUFLOW also revealed a 24.97km$^2$ inundation extent for a 2-year return period, 27.87km$^2$ inundation extent for a 5-year period and 26.10km$^2$ inundation extent for a 10-year return period, increasing to its peak extent by 3.67% by the 5-year return period, then decreasing by 2.24% by the 10-year return period. The flood frequency return as modeled by Flood Modeler indicated a 25.04km$^2$ inundation extent for a 2-year return period, 28.10km$^2$ inundation extent for a 5-year period and 26.04km$^2$ inundation extent for a 10-year return period. Increasing to its peak extent by 3.67% by the 5-year return period, and then decreased by 2.24% by the 10-year return period. The surface runoff potential revealed that 35.99% with an area of 1630.19 km$^2$ had low infiltration potential, 32.51% with an area of 1472.56 km$^2$ had moderate infiltration, while 31.50% with an area of 1426.82 km$^2$ had high infiltration. This indicated that the study area had a great extent of low surface infiltration, which will lead to flooding during heavy or frequent rainfalls. These results indicated that out of the three models tested, HecRAS had the best fit to the ground flood points, and it was recommended to be used as a hydraulic flood modeling option.*

***Keywords*** *- Flood Vulnerability, GIS, Hydraulic Modelling, Surface Runoff, Hec-RAS, Tuflow, Flood Modeler.*

## 1. Introduction

Flooding is one of the major environmental hazards affecting many communities across the world, with serious effects on the environment and the well-being of the population. Nigeria has experienced repeated flood events associated with changing rainfall conditions, settlement expansion and the occupation of natural drainage corridors and floodplains [1-3]. Climate change has also contributed to changes in rainfall intensity and hydrological conditions, thereby increasing the occurrence and severity of flooding in downstream parts of the country [4]. Floods usually occur when runoff generated from rainfall exceeds the capacity of rivers, streams and drainage channels, causing water to spread into surrounding land [5, 6].

Flooding may also result from coastal storm surges, tidal processes and sea-level rise. Poor waste disposal, blocked drainage systems, and the development of settlements within floodplains further increase flood problems in many Nigerian towns and cities [3,7].

Flood management measures depend on the ability to predict the movement of floodwater and identify areas that will be inundated. Flood parameters such as inundation extent, water depth, flow velocity and flood duration can be simulated to support emergency response, infrastructure planning and disaster management [2]. Hydraulic modelling now provides useful methods for analysing drainage conditions and representing the spatial behaviour of floodwater under different hydrological events [8,9].

Several hydraulic models are available for flood simulation and inundation mapping, including HEC-RAS, TUFLOW and Flood Modeller. HEC-RAS was developed by the Hydrologic Engineering Center of the United States Army Corps of Engineers. The software is capable of carrying out one-dimensional and two-dimensional steady and unsteady flow simulations. It also contains facilities for data management, hydraulic computation, mapping and the presentation of model results. Its integration with GIS has encouraged its application in river and floodplain studies.

TUFLOW is a one-dimensional and two-dimensional hydraulic model designed for the simulation of flood and tidal processes. The model is suitable for rivers, floodplains, estuaries, coastal waters and urban drainage systems where water movement may be difficult to represent using only a one-dimensional channel network. It can be used to model river flooding, overland flow, urban drainage and interactions between channels and adjoining floodplains.

Flood Modeller is a hydraulic modelling program developed by Jacobs for simulating water movement through river channels and across floodplains. It uses one-dimensional and two-dimensional hydraulic solvers and provides a GIS-based interface for constructing models, running simulations and displaying flood results. HEC-RAS, TUFLOW and Flood Modeller therefore have related functions, although they differ in numerical procedures, data requirements, computational structure and the manner in which river and floodplain processes are represented [2].

Scientists and engineers have continued to develop hydraulic models capable of providing improved representations of flow within rivers, channels and floodplains. Model performance, however, depends not only on the number of processes represented but also on the quality of the input data, model calibration, terrain characteristics, boundary conditions and the nature of flooding within the study area. A complex model may therefore not always produce a more accurate result than a simpler model when the available data are limited or when the model is not suited to local conditions.

Although hydraulic modelling is increasingly being used for flood assessment in Nigeria, few studies have directly compared the accuracy and applicability of different hydraulic models under the same hydrological and environmental conditions [10,11]. This creates uncertainty in selecting an appropriate model for flood mapping, particularly where several modelling packages produce similar outputs but require different levels of data, calibration and computation. Hence, this study seeks to evaluate and compare the performance of HEC-RAS, TUFLOW and Flood Modeller for flood vulnerability assessment under identical hydrological and environmental conditions.

### *1.1. Study Area*

Abia is a state in the south-eastern part of Nigeria, located between latitude $5^0$ 00'N and $6^0$ 00'N and longitude $7^0$ 00'E and $8^0$ 00'E of the equator, see Figure 1. It occupies about 6,320 square kilometers and is bounded on the north by Enugu, west by Imo State, east by Akwa Ibom and to the south by Rivers State. The southern part of the State lies within the riverine part of Nigeria, which is a low-lying rainforest. The southern portion gets heavy rainfall of about 2,400 millimeters (94 in) per year, especially intense between the months of April and October. The rest of the State is moderately high plain and wooded savanna, and the most important rivers are the Imo and Aba Rivers, which flow into the Atlantic Ocean through Akwa Ibom State.

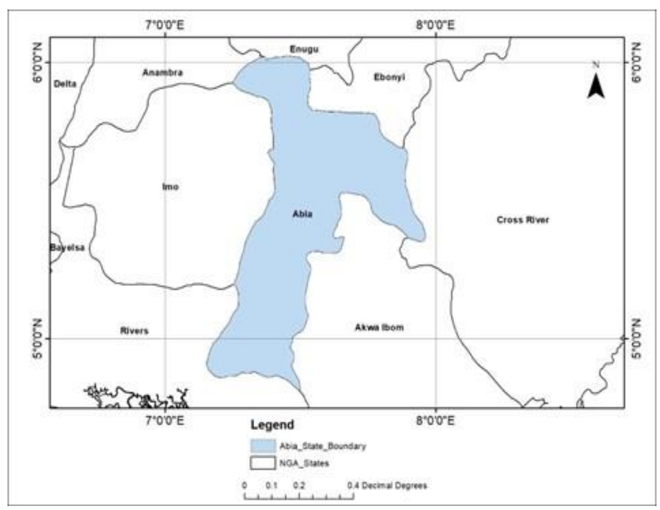


**Fig. 1 Location Maps of the study area**

## 2. Material and Methodology

This paper used both remotely sensed data and ancillary geospatial datasets to carry out hydraulic flood modelling and analysis within the study area. The main datasets comprised Sentinel-2A multispectral satellite imagery acquired in 2018 and the ALOS PALSAR Digital Elevation Model (DEM). Both datasets were downloaded from the United States Geological Survey (USGS) Earth Explorer platform. The Sentinel-2A imagery was used to generate the land use and land cover map, whereas the ALOS PALSAR DEM served as the basis for terrain analysis, watershed delineation, extraction of river geometry, and the derivation of hydraulic parameters required for flood modelling.

Additional spatial datasets were obtained to define the geographical extent of the study area and support geospatial analysis. The administrative boundary map of Nigeria was obtained from the QGIS 1.8.0 Lisboa Tutorial Package, while the administrative boundary of Abia State was sourced from the Department of Surveying and Geoinformatics, Nnamdi Azikiwe University, Awka. These datasets were used to clip the satellite imagery and elevation data to the study area, establish a common spatial reference, and prepare the datasets for subsequent analysis. Rainfall information used in the hydrological component of the study was obtained from the Nigerian Meteorological Agency (NIMET). The rainfall records provided the precipitation characteristics required to generate model inputs and simulate flood conditions within the study area.

A number of software applications were used throughout the study to process the datasets, perform spatial analysis, and run the hydraulic simulations. HEC-RAS, TUFLOW, and Flood Modeller were employed to simulate flood behaviour and evaluate inundation patterns under different hydraulic modelling approaches. ArcGIS 10.6 was used for spatial analysis, geoprocessing, and map production, while ERDAS Imagine 9.1 was used for satellite image processing, land use and land cover classification, and raster-based analysis.

## 3. Discussion of Results

### *3.1. Elimination of Outliers*

In order to remove the outliers in the DEM data, the extract sample tool of the spatial analyst tool of Arc GIS 10.7 software was used to extract common points among the DEM and the ground reference points. The ground reference point was selected as the input point file, while the DEM dataset was selected as the input raster data. A random sampling technique was used to extract the points. A total of 700 points were extracted, and outliers were detected and removed. A total of 600 points were remaining after removing the outliers.

### *3.2. Ground Validation of ALOS PALSAR DEM using Ground Control Points*

In order to use the ALOS PALSAR DEM in flood modelling in Abia State, the DEM had to be validated first using ground control points on the ground. The elevation points obtained from the ALOS PALSAR DEM were compared with the elevation points collected from ground controls. The result is illustrated in Figure 2.

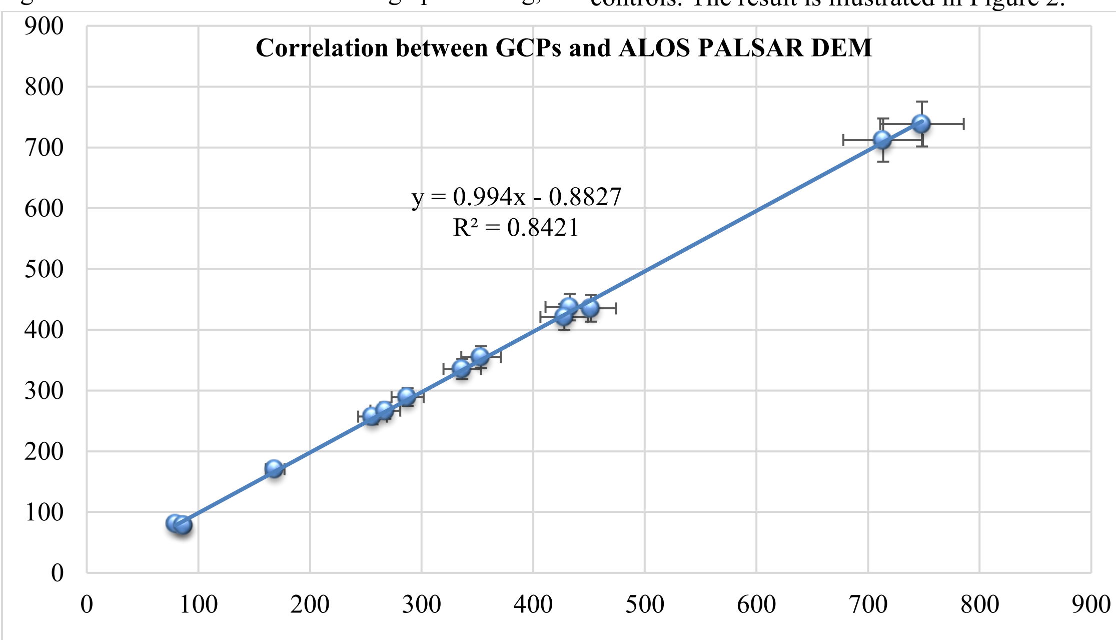


**Fig. 2 Correlation between GCP and ALOS PALSAR DEM**

From Figure 2, the correlation results gave a value of 0.8421, which indicates a strong positive relationship between the ground control points and the elevation points from ALOS PALSAR DEM. This means that the DEM is a good fit and represents the elevation values on the ground.

### *3.3. Analysis of Vertical and Horizontal Accuracy using Root Mean Square Error (RMSE)*

RMSE for DEM vertical accuracy is defined as:

$$\sqrt{\frac{\sum(Z_R-Z_S)^2}{n}} \quad (1)$$

where $Z_i$ is the interpolated DEM elevation of a test point and $Z_t$ is the true elevation of a test point, and n is the number of test points. RMSE for ALOS PALSAR vertical accuracy is given as:

$$\sum(ZR - ZS) = 7647.989$$

where

$Z_S$= elevation points of ALOS PALSAR
$Z_R$ = elevation points of GCPS
$\frac{\sum(Z_R-Z_S)^2}{n} = \frac{7647.989}{240} = 31.86$
$RMSE = \sqrt{\frac{\sum(Z_R-Z_S)^2}{n}} = \sqrt{31.86} = 5.64$

Table 2 shows the summary of vertical accuracy for the elevation dataset under study.

**Table 2. Summary of vertical accuracy of the DEM**

| S/N | DEM | VERTICAL RMSE (m) |
|---|---|---|
| 1 | Alos Palsar | 5.64m |

According to the Federal Geographic Data Committee (FGDC), horizontal accuracy is determined through the calculation of RMSE with the following formula:

$$RMSEr = RMSEx2 + RMSEy2$$

where

$$RMSE_x = \sqrt{\frac{\sum_{i=1}^{n}\left(X_{Ref,i} - X_{Study,i}\right)^2}{n}}$$

and

$$RMSE_y = \sqrt{\frac{\sum_{i=1}^{n}\left(Y_{Ref,i} - Y_{Study,i}\right)^2}{n}}$$

where:
$X_{Ref}$ = Easting coordinate of the reference Ground Control Point (GCP)
$X_{Study}$ = Easting coordinate extracted from the DEM under evaluation
$Y_{Ref}$ = Northing coordinate of the reference Ground Control Point (GCP)
$Y_{Study}$= Northing coordinate extracted from the DEM under evaluation
$n$ = Total number of Ground Control Points (GCPs) used in the accuracy assessment

For ALOS PALSAR, the horizontal RMSE was calculated as follows:

$$RMSEx = \sqrt{\frac{1989.41}{20}}$$
$$= \sqrt{99.47}$$
$$= 9.97\ m$$

where
$n = 20$ is the total number of check points used for the accuracy assessment.

Similarly,

$$RMSEy = \sqrt{\frac{\sum(Y_R - Y_S)^2}{n}}$$
$$= \sqrt{\frac{2146.45}{20}}$$
$$= \sqrt{107.32}$$
$$= 10.36\ m$$

The horizontal Root Mean Square Error (RMSE) is then computed as:

$$RMSE_r = \sqrt{RMSE_x^2 + RMSE_y^2}$$
$$= \sqrt{(9.97)^2 + (10.36)^2}$$
$$= \sqrt{206.79}$$
$$= 14.39\ m$$

The results of horizontal accuracy are summarized in Table 3.

**Table 3. Summary of horizontal accuracy of the DEM**

| S/N | DEM | HORIZONTAL RMSE (m) |
|---|---|---|
| 1 | ALOS PALSAR | 14.39 |

The acceptability of hydrologic delineations depends greatly on the user's need. Delineation accuracy values cannot be expected to be much greater than the cell resolution of the DEM from which they were produced (Ejikeme, 2015). Gamett (2010) stated that an accuracy threshold of 30 meters for quantitative comparison of ASTER, NED and SRTM, Alos Palsar DEMs is deemed acceptable. Once DEM accuracy meets an acceptable tolerance, hydrologic data derived from the model can also be assumed to be more accurate (Srivastava, 2000).

### *3.4. Landcover/landuse of Abia State in 2018*

The landcover/landuse distribution of Abia State in 2018, as shown in Figure 3 and Table 4, indicates that grassland accounted for the largest land cover/use of about 52.06% and an area of about 2459.28 km$^2$. Urban area had 23.21% and a coverage area of 1096.41 km$^2$, forest had 18.36% with an area of 867.44 km$^{2,}$ and water body had the lowest turnout with 6.35% with an area of 300.32 km$^2$.

**Table 4. LULC distribution for Abia State**

| Class Name | Area(km$^2$) | Percentage (%) |
|---|---|---|
| Urban area | 1096.41 | 23.21 |
| Grassland | 2459.28 | 52.06 |
| Forest | 867.44 | 18.36 |
| Water body | 300.32 | 6.35 |
| Total | 4723.45 | 100 |

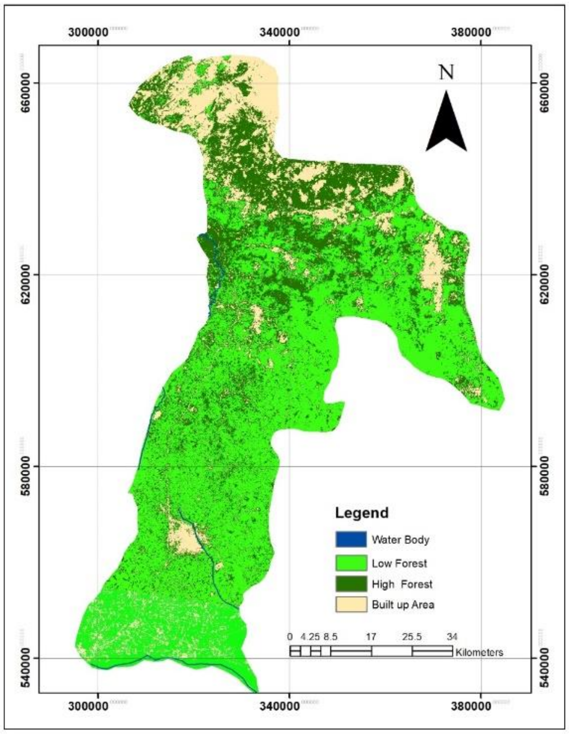


**Fig. 3 Landcover/landuse of Abia State**

A confusion matrix was calculated to determine the accuracy of the landcover/landuse classification. The precision of the classified images was ascertained, and an accuracy assessment was carried out by comparing the classified Landsat image with known reference pixels. A table for accuracy assessment was prepared, as shown in Table 5.

**Table 5. Accuracy Assessment**

| Class | Producer's Accuracy (%) | User's Accuracy (%) | Kappa |
|---|---|---|---|
| Built-up Area | 90.41 | 95.65 | 0.9461 |
| Grassland | 83.75 | 82.71 | 0.9595 |
| Forest | 100.00 | 100.00 | 0.9520 |
| Water Body | 100.00 | 100.00 | 1.0000 |
| Overall Accuracy | 92.18% | | 0.9534 |

In Table 4, the total number of reference points used was 256 and total number of points classified was 256, and the total number of correctly classified points was 236. The overall classification accuracy gotten was 96.88%, and the overall kappa was 0.9218.

### *3.5. Surface Runoff Modelling*

Surface runoff is the flow of water that occurs when excess stormwater flows over the ground surface. This can occur when the soil is saturated to full capacity, and rain arrives more quickly than the soil can absorb it (Keith and Robert, 2004). In the study, the landcover/landuse map, rainfall data and soil map were used to model the surface runoff potential in Abia state. The landcover/landuse map, soil map and rainfall data were first used to derive the curve number map, the curve number being one of the major governing factors that predominantly affect the runoff amount that flows over the land after satisfying all losses, which plays an important role in defining the hydrological response of the catchment.

Zero curve number describes the hydrological response only with infiltration. All the rainfall water will infiltrate to become subsurface flow. When the Curve Number is 100, it describes the hydrological responses with no infiltration. All the rainfall water will flow as surface flow as the soil is in saturation limit that happens in continuous rainfall events. If CN increased, the runoff from that watershed would also increase. The runoff potential map was created from the curve number, as shown in Figure 4.

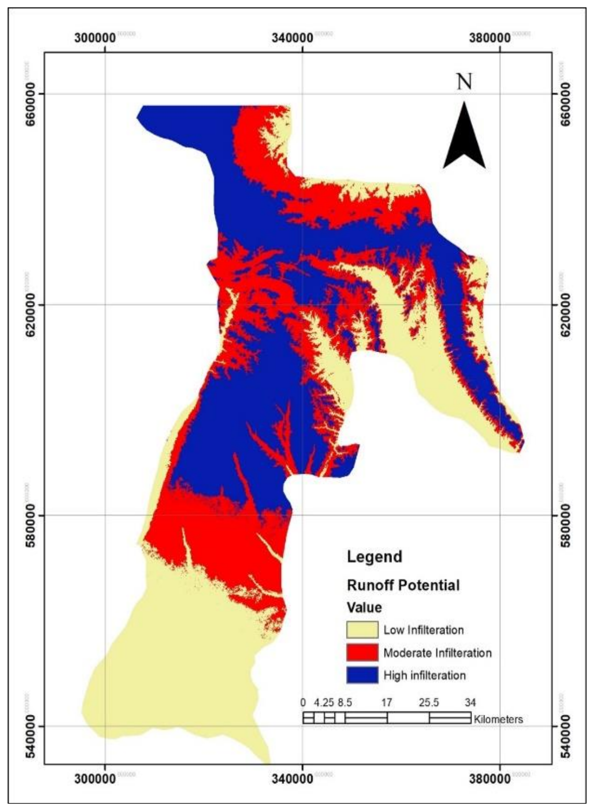


**Fig. 4 Surface runoff potential in Abia State**

The surface runoff potential in Figure 4 revealed that 35.99% with an area of 1630.19 $km^2$ had low infiltration potential, 32.51% with an area of 1472.56 $km^2$ had moderate infiltration, while 31.50% with an area of 1426.82 $km^2$ had high infiltration. This indicated that a large portion of the study area has a high potential for low surface infiltration, which will lead to flooding during rainfalls.

### ***3.6. Flood Frequency Analysis***

Flood frequency is a multidimensional tool used in the assessment of water resource potential as well as a measure of both hydrologic and hydraulic measures. It provides the data frame for inundation area mapping as well as for the assessment of flood hazard and risk within an area. The flood frequencies of Abia State were modelled using HEC-RAS, TUFLOW and flood modeler, and the results are shown in Figures 5, 6 and 7.

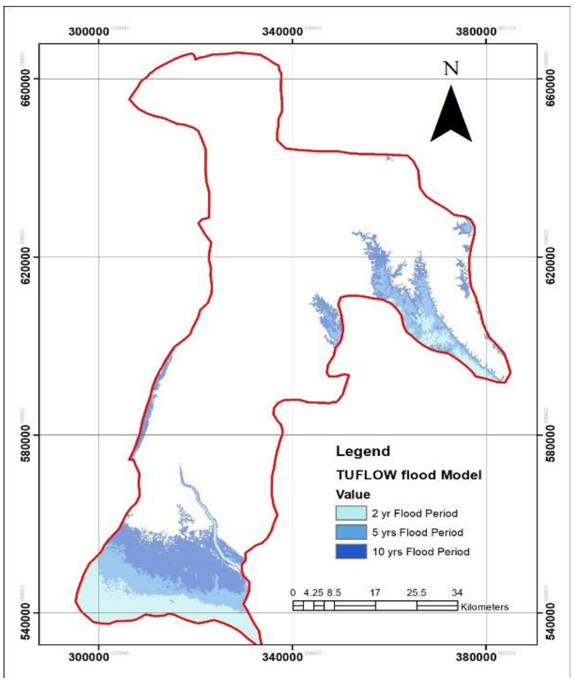


**Fig. 5 Flood frequency as modeled by HEC-RAS**

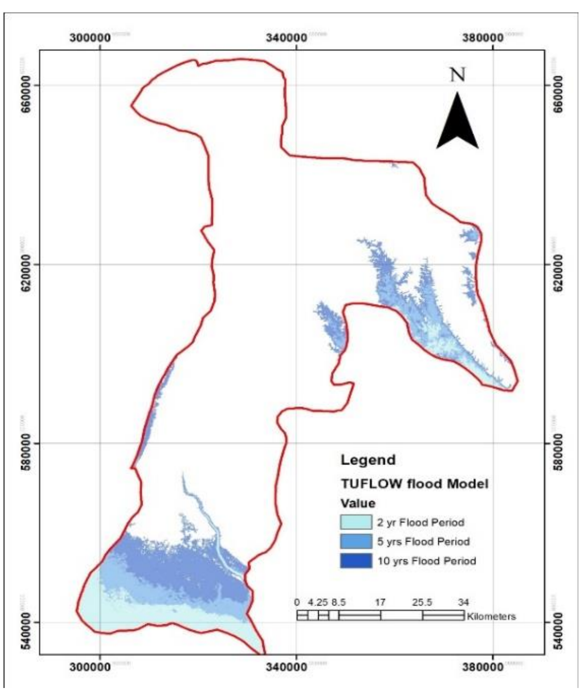


**Fig. 6 Flood frequency as modeled by TUFLOW**

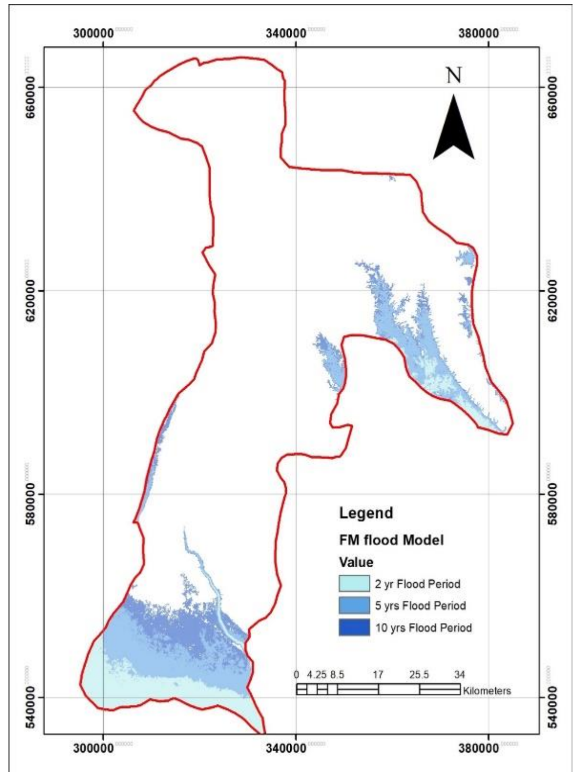


**Fig. 7 Flood frequency as modeled by the flood modeler**

The results from the HEC-RAS model (Figure 8) indicated that the inundation extents for a 10-year return period were given as 25.43km$^2$ inundation extent for a 2-year return period, 28.09km$^2$ inundation extent for a 5-year period and 26.67km$^2$ inundation extent for a 10-year return period. The flood extent as modeled by HEC-RAS increased by the fifth-year return period by 3.15%, then decreased by 1.8% by the tenth-year return period. The peak inundation extent was reached at the 5-year return period. This is illustrated in Table 6.

**Table 6. HEC-RAS model flood frequency**

| HEC-RAS | Extent(Km$^2$) | Percentage |
|---|---|---|
| 2-year return period | 25.43 | 32.18% |
| 5-year return period | 28.09 | 35.55% |
| 10-year return period | 26.67 | 33.75% |
| Total | 80.19 | 100 |

The results from the TUFLOW model (Figure 9) indicated that the inundation extents for a 10-year return period were given as 24.97km$^2$ inundation extent for a 2-year return period, 27.87km$^2$ inundation extent for a 5-year period and 26.10km$^2$ inundation extent for a 10-year return period. The flood extent as modeled by TUFLOW increased by the fifth-year return period by 3.67%, then decreased by 2.24% by the tenth-year return period. The peak inundation extent was also reached at the 5-year return period. This is illustrated in Table 7.

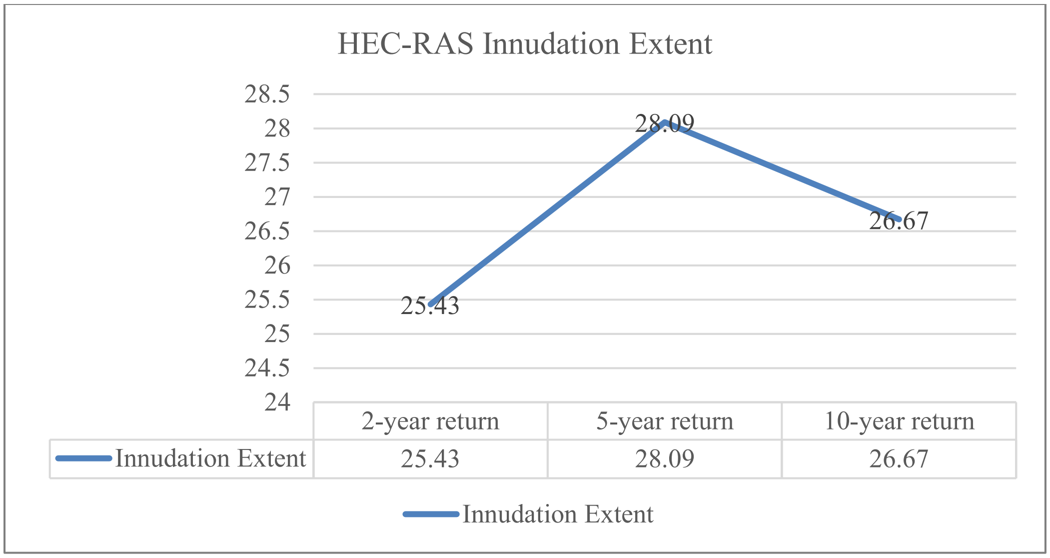


**Fig. 8 Graph showing HEC-RAS modeled flood extent for 2yr, 5yr, 10yr returns**

**Table 7. TUFLOW model flood frequency**

| TUFLOW | Extent ($Km^2$) | Percentage |
|---|---|---|
| 2-year return period | 24.97 | 31.63% |
| 5-year return period | 27.87 | 35.30% |
| 10-year return period | 26.10 | 33.06% |
| Total | 78.94 | 100 |

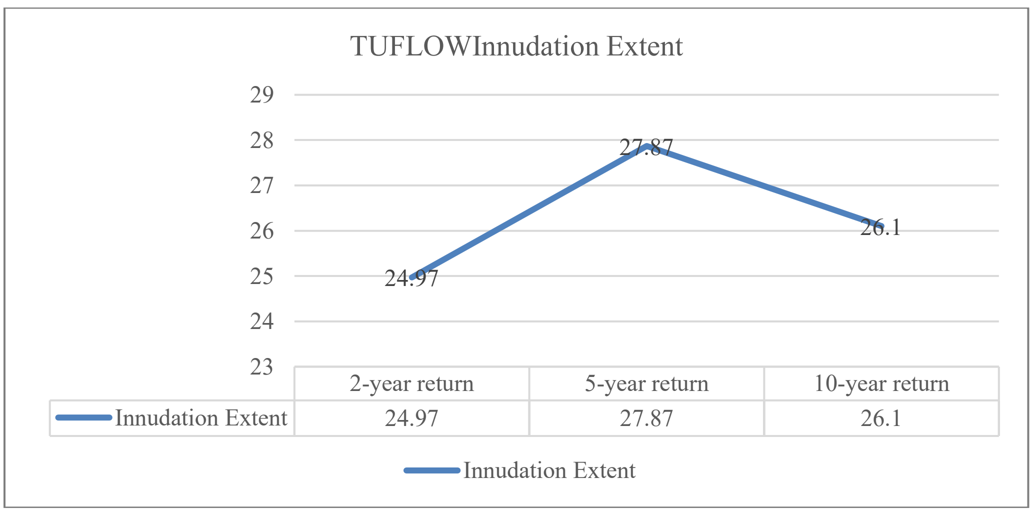


**Fig. 9 Graph showing TUFLOW modeled flood extent for 2yr, 5yr, 10yr returns**

The results from the flood modeler (Figure 10) indicated that the inundation extents for a 10-year return period were given as 25.04km$^2$ inundation extent for a 2-year return period, 28.10km$^2$ inundation extent for a 5-year period and 26.04km$^2$ inundation extent for a 10-year return period. The flood extent as modeled by the flood modeler increased by the fifth-year return period by 3.67%, then decreased by 2.24% by the tenth-year return period. The peak inundation extent was also reached at the 5-year return period. This is illustrated in Table 8.

**Table 8. Flood modeler flood frequency**

| Flood modeler | Extent ($Km^2$) | Percentage |
|---|---|---|
| 2-year return period | 25.04 | 32.02% |
| 5-year return period | 28.10 | 35.94% |
| 10-year return period | 26.04 | 33.30% |
| Total | 78.18 | 100 |

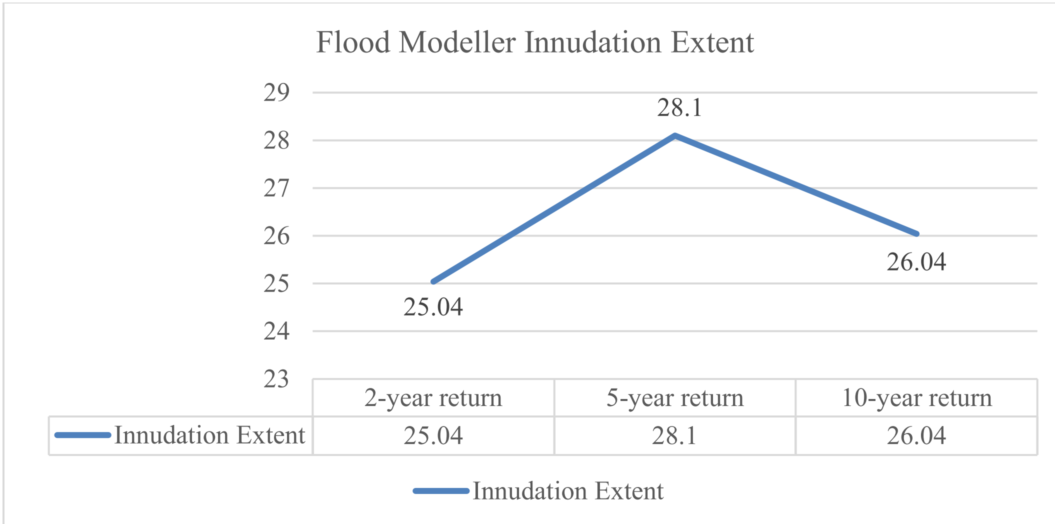


**Fig. 10 Graph showing flood modeler flood extent for 2yr, 5yr, 10yr returns**

### *3.7. Flood Vulnerability Mapping*

The results of the vulnerability modelling with HEC-RAS, TUFLOW and Flood Modeler produced each a layer showing four vulnerable zones; namely, very high risk, high risk, moderate risk and low risk flood zones in the study area.

The results obtained from the HEC-RAS modelled vulnerability revealed very high-risk zone occupied 9.77% of the entire study area, covering an area of 442.59$km^2$, while high risk zone occupied 28.08%, covered an area of 1272$km^2$. The moderate risk zone occupied 32.92%, covering 1491.58 $km^{2,}$ while the low risk zone occupied 29.21%, covering an area of 1323.42 $km^2$. The TUFLOW modelled vulnerability revealed that a very high-risk zone occupied 9.72% of the entire study area, covering an area of 440.59$km^2$, while high risk zone occupied 27.59%, covered an area of 1250.03$km^2$. The moderate risk zone occupied 33.02%, covering 1491.58 $km^{2,}$ while the low risk zone occupied 29.65%, covering an area of 1343.39 $km^2$. The flood modeler modelled vulnerability revealed that the very high-risk zone occupied 9.69% of the entire study area, covering an area of 439.10$km^2$, while high risk zone occupied 27.87%, covered an area of 1262.53$km^2$. The moderate risk zone occupied 32.87%, covering 1489.25$km^2$ while the low risk zone occupied 29.55%, covering an area of 1338.71$km^2$. This distribution is also represented in Table 9 and Figure 11.

**Table 9. Flood vulnerability distribution**

| Risk Class | HEC-RAS ($km^2$) | TUFLOW ($km^2$) | Flood Modeler ($km^2$) |
|---|---|---|---|
| Very High | 442.59 | 440.01 | 439.10 |
| High | 1,272.00 | 1,250.03 | 1,262.53 |
| Moderate | 1,491.58 | 1,495.58 | 1,489.25 |
| Low | 1,323.42 | 1,343.39 | 1,338.71 |
| Total | 4,529.59 | 4,529.59 | 4,529.59 |

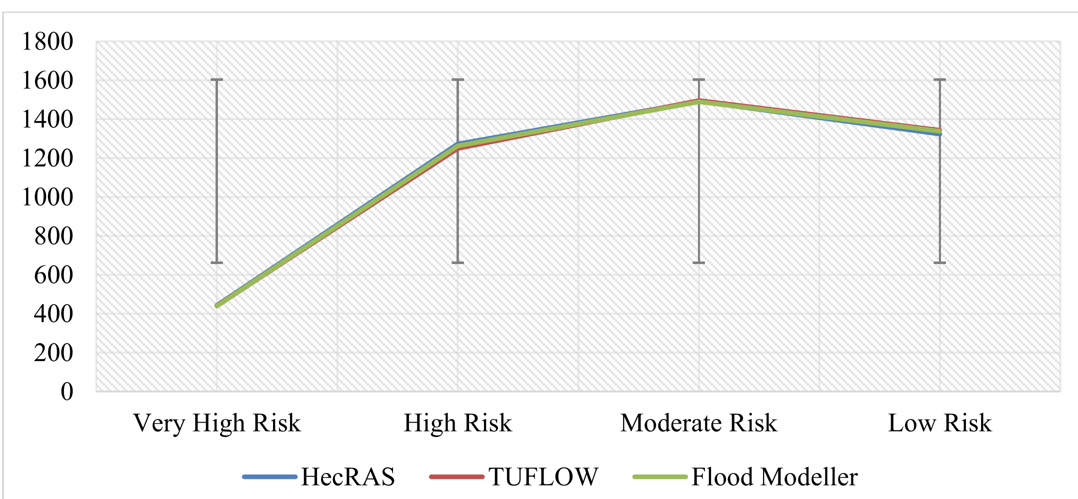


**Fig. 11 Flood Distribution gotten from Hec-RAS, TUFLOW and Flood Modeller**

*3.7.1. Features at Very High-Risk Flooding as Modeled by HEC-RAS*

An overlay analysis was done, overlaying the flood risk layer with the landcover/landuse layer to determine areas at risk as modeled by HEC-RAS.

The results showed that built up area had 34.59% with an area of 153.12km$^2$ in the very high-risk area, while the high forest had 30.70% and an area of 135.89km$^2$, the low forest had 23.37% with an area of 103.45 km$^{2,}$ and the waterbody had 11.32% with an area of 50.13 km$^2$. The distribution of class within the very high-risk flood zone is shown in Table 10 and Figure 12.

**Table 10. Very high-risk distribution zone**

| S/N | Class Name | Area (km$^{2)}$ | Percentage |
|---|---|---|---|
| 1 | Built-up area | 153.12 | 34.59 |
| 2 | High Forest | 135.89 | 30.70 |
| 3 | Low Forest | 103.45 | 23.37 |
| 4 | Waterbody | 50.13 | 11.32 |
| | Total | 442.59 | 100 |

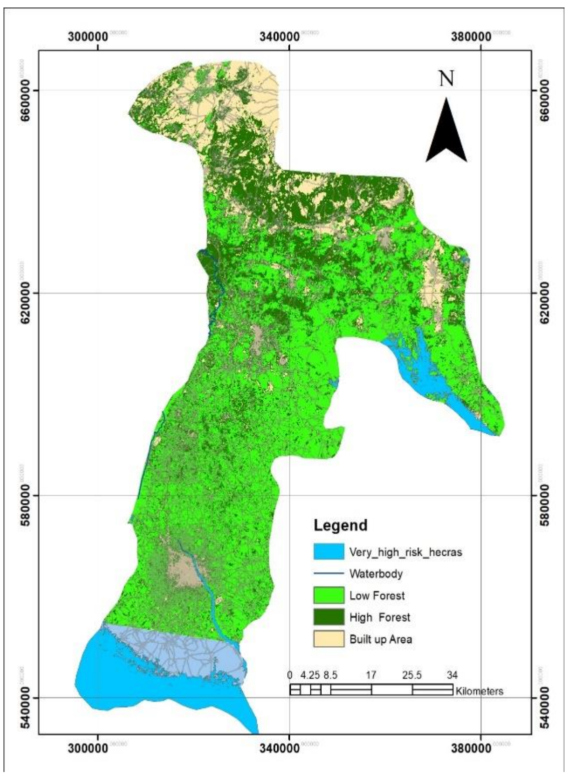


**Fig. 12 Very high-risk zone as modeled by HEC-RAS**

*3.7.2. Features at high-risk flooding as modeled by HEC-RAS*

The results showed that built up area had 47.21% with an area of 600.56km$^2$ in the high-risk area, while the high forest had 19.40% and an area of 246.78km$^2$, the low forest had 27.34% with an area of 347.8km$^2$ and the waterbody had 6.04% with an area of 76.86km$^2$. The distribution of class within the high-risk flood zone is shown in Table 11 and Figure 13.

**Table 11. Distribution of feature class at high-risk zone**

| S/N | Class Name | Area | Percentage |
|---|---|---|---|
| 1 | Built-up area | 600.56 | 47.21 |
| 2 | High Forest | 246.78 | 19.40 |
| 3 | Low Forest | 347.8 | 27.34 |
| 4 | Waterbody | 76.86 | 6.04 |
| | Total | 1272.00 | 100.00 |

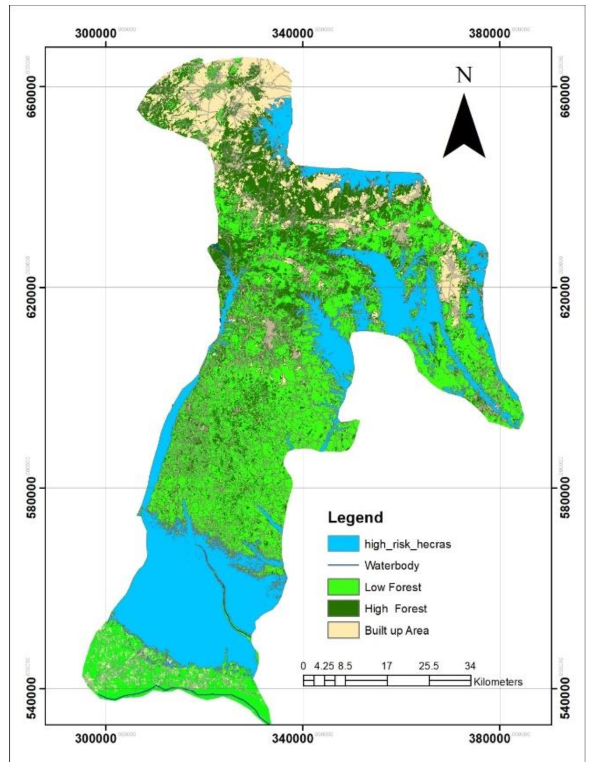


**Fig. 13 High-risk zone as modeled by HEC-RAS**

*3.7.3. Features at Risk of Moderate Risk Flooding as Modelled by HEC-RAS*

The results showed that built up area had 49.42% with an area of 737.22km$^2$ in the moderate-risk area, while the high forest had 26.15% and an area of 390.09km$^2$, the low forest had 19.99% with an area of 298.21km$^2$ and the waterbody had 4.42% with an area of 66.06 km$^2$. The distribution of class within the moderate risk flood zone is shown in Table 12 and Figure 14.

**Table 12. Distribution of feature class at moderate risk**

| S/N | Class Name | Area | Percentage |
|---|---|---|---|
| 1 | Built-up area | 737.22 | 49.42 |
| 2 | High Forest | 390.09 | 26.15 |
| 3 | Low Forest | 298.21 | 19.99 |
| 4 | Waterbody | 66.06 | 4.42 |
| | TOTAL | 440.59 | 100 |

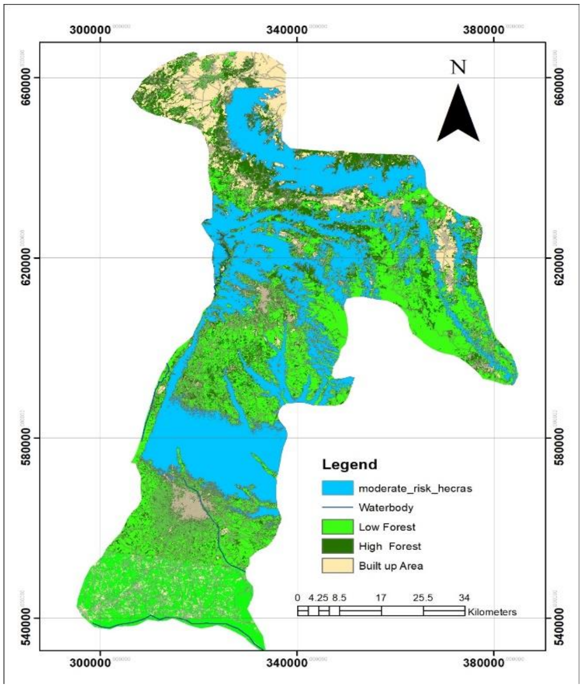


**Fig. 14 Moderate-risk zone as modeled by HEC-RAS**

*3.7.4. Features at Low risk as modelled by HEC-RAS*

The results showed that built up area had 44.73% with an area of 592.06km$^2$ in the low-risk area, while the high forest had 27.45% and an area of 363.29km$^2$, the low forest had 25.01% with an area of 331.11km$^2$ and the waterbody had 2.79% with an area of 36.96 km$^2$. The distribution of class within the low-risk zone is shown in Table 13 and Figure 15.

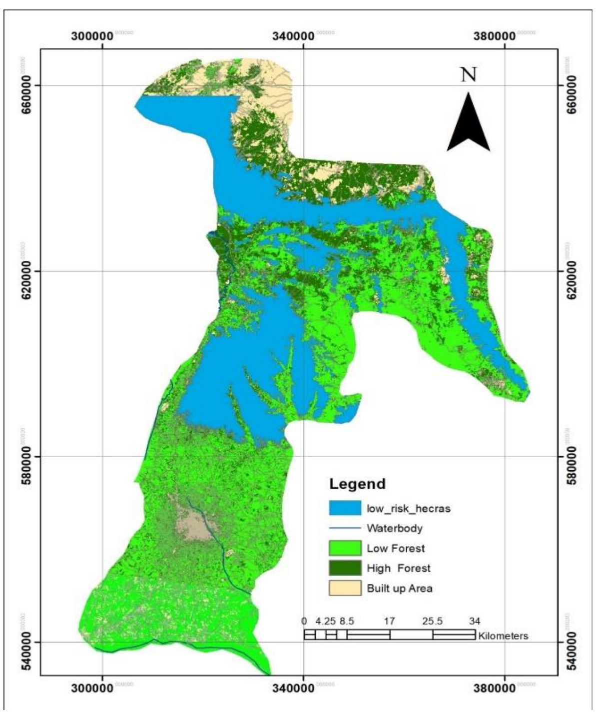


**Fig. 15 Low-risk zone as modeled by HEC-RAS**

**Table 13. Distribution of feature class at low-risk flooding**

| S/N | Class Name | Area | Percentage |
|---|---|---|---|
| 1 | Built-up area | 592.06 | 44.73 |
| 2 | High Forest | 363.29 | 27.45 |
| 3 | Low Forest | 331.11 | 25.01 |
| 4 | Waterbody | 36.96 | 2.79 |
| | TOTAL | 1323.42 | 100 |

*3.7.5. Features at very High-Risk Zone as modeled by TUFLOW*

The results showed that built up area had 34.59% with an area of 153.12km$^2$ in the very high-risk area, while the high forest had 30.70% and an area of 135.89km$^2$, the low forest had 23.37% with an area of 103.45km$^2$ and the waterbody had 11.32% with an area of 48.13km$^2$. The distribution of class within the very high-risk zone is shown in Table 14 and Figure 16.

**Table 14. Distribution of feature class at low risk flooding**

| S/N | Class Name | Area (km$^{2)}$ | Percentage |
|---|---|---|---|
| 1 | Built-up area | 153.12 | 34.75 |
| 2 | High Forest | 135.89 | 30.84 |
| 3 | Low Forest | 103.45 | 23.47 |
| 4 | Waterbody | 48.13 | 10.92 |
| | Total | 440.59 | 100 |

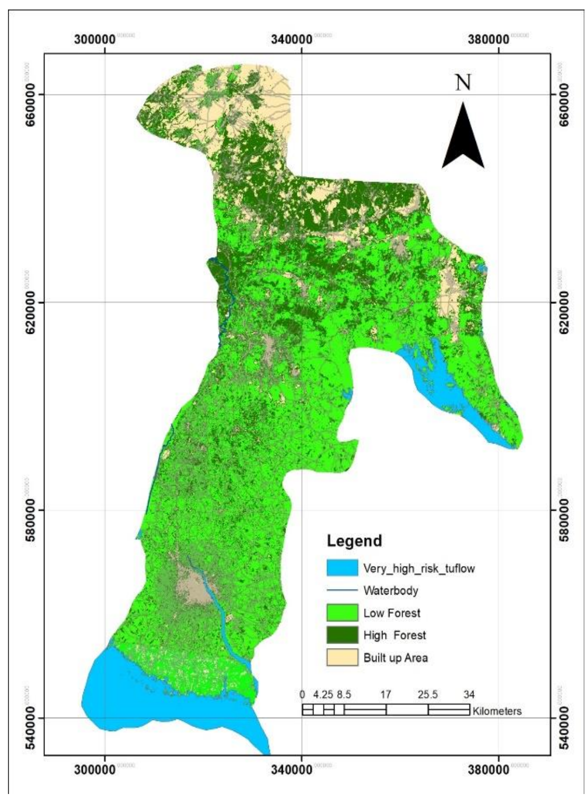


**Fig. 16 Very high-risk zone as modeled by TUFLOW**

### *3.7.6. Features at High-Risk Flooding as Modelled by TUFLOW*

The results showed that built up area had 46.44% with an area of 580.53km$^2$ in the high-risk area, while the high forest had 19.74% and an area of 246.78km$^2$, the low forest had 27.90% with an area of 347.8km$^2$ and the waterbody had 6.14% with an area of 76.86km$^2$. The distribution of class within the high-risk flood zone, as modeled by TUFLOW, is shown in Table 15 and Figure 17.

**Table 15. Distribution of feature class at risk of high-risk flooding**

| S/N | Class Name | Area | Percentage |
|---|---|---|---|
| 1 | Built-up area | 580.53 | 46.44 |
| 2 | High Forest | 246.78 | 19.74 |
| 3 | Low Forest | 347.8 | 27.90 |
| 4 | Waterbody | 76.86 | 6.14 |
| | Total | 1250.03 | 100.00 |

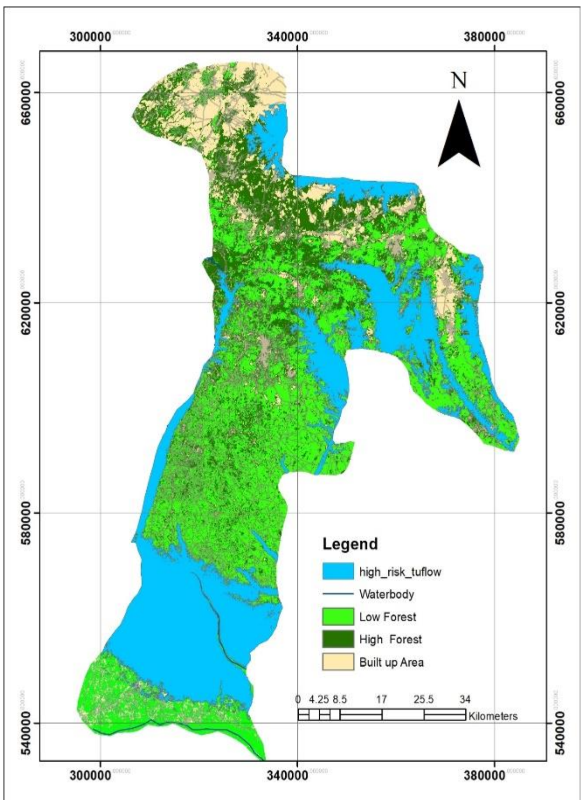


**Fig. 17 High-risk zone as modeled by TUFLOW**

### *3.7.7. Features at Moderate Risk of Flooding as Modelled by TUFLOW*

The results showed that built up area had 49.62% with an area of 742.22km$^2$ in the moderate-risk area, while the high forest had 26.08% and an area of 390.09km$^2$, the low forest had 19.93% with an area of 298.21km$^2$ and the waterbody had 4.42% with an area of 66.06 km$^2$. The distribution of class within the moderate risk flood zone is shown in Table 16 and Figure 18.

**Table 16. Distribution of feature class at moderate risk**

| S/N | Class Name | Area | Percentage |
|---|---|---|---|
| 1 | Built-up area | 742.22 | 49.62 |
| 2 | High Forest | 390.09 | 26.08 |
| 3 | Low Forest | 298.21 | 19.93 |
| 4 | Waterbody | 66.06 | 4.42 |
| | TOTAL | 1495.58 | 100 |

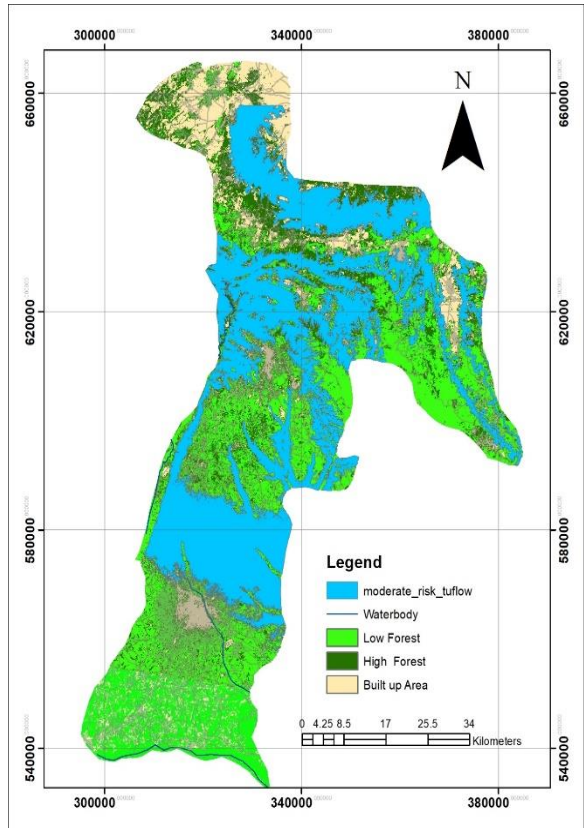


**Fig. 18 Moderate-risk zone as modeled by TUFLOW**

### *3.7.8. Features at Risk of Low Risk Zone as Modelled by TUFLOW*

The results showed that built up area had 44.81% with an area of 602.06km$^2$ in the low-risk area, while the high forest had 27.78% and an area of 373.29km$^2$, the low forest had 25.39% with an area of 341.11km$^2$ and the waterbody had 2.00% with an area of 29.96 km$^2$.

The distribution of class within the moderate risk flood zone is shown in Table 17 and Figure 19.

**Table 17. Distribution of feature class at low-risk flooding**

| S/N | Class Name | Area | Percentage |
|---|---|---|---|
| 1 | Built Up Area | 602.06 | 44.81 |
| 2 | High Forest | 373.29 | 27.78 |
| 3 | Low Forest | 341.11 | 25.39 |
| 4 | Waterbody | 26.96 | 2.00 |
| | Total | 1343.42 | 100 |

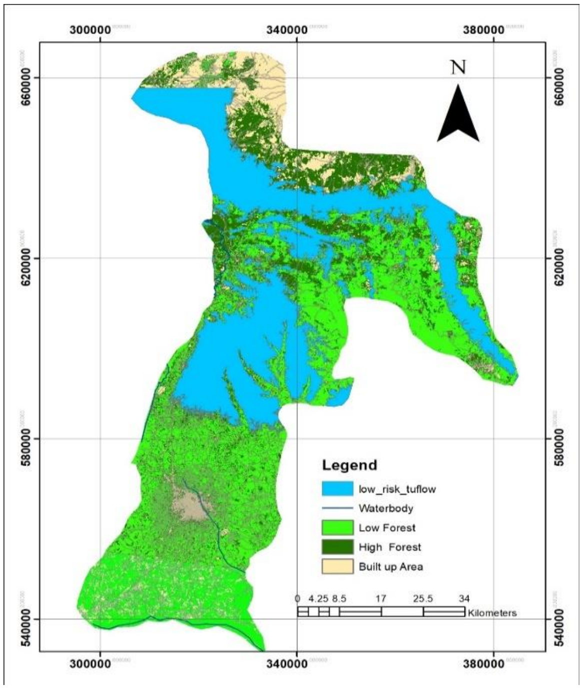


Fig. 19 Low-risk zone as modeled by TUFLOW

*3.7.9. Features at very High-Risk Flooding as modeled by Flood Modeler*

The results showed that built up area had 34.64% with an area of 152.12km$^2$ in the very high-risk area, while the high forest had 30.94% and an area of 135.89km$^2$, the low forest had 23.55% with an area of 103.45km$^2$ and the waterbody had 10.96% with an area of 48.13km$^2$.

The distribution of class within the very high-risk zone is shown in Table 18 and Figure 20.

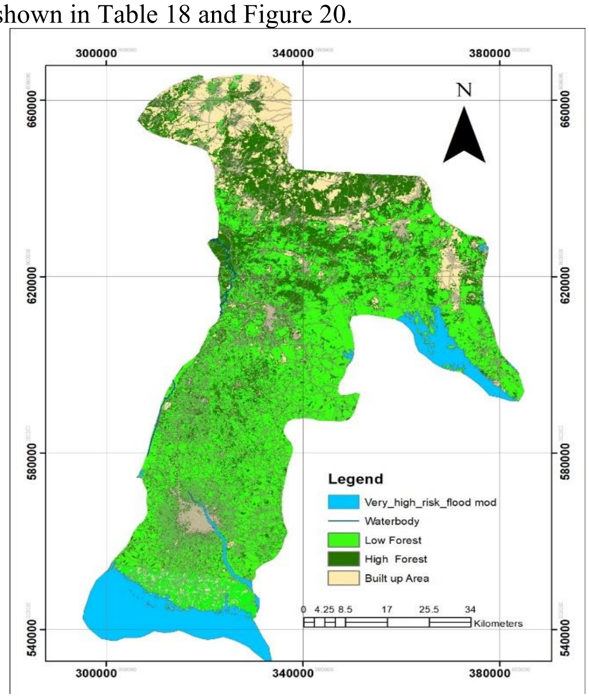


Fig. 20 Very high-risk zone as modeled by flood modeler

**Table 18. Distribution of feature class at very high risk of flooding**

| S/N | Class Name | Area (km$^{2)}$ | Percentage |
|---|---|---|---|
| 1 | Built up area | 152.12 | 34.64 |
| 2 | High Forest | 135.89 | 30.94 |
| 3 | Low Forest | 103.45 | 23.55 |
| 4 | Waterbody | 48.13 | 10.96 |
| | Total | 439.10 | 100 |

*3.7.10. Features at High-Risk Flooding*

The results showed that built up area had 44.70% with an area of 564.43km$^2$ in the high-risk area, while the high forest had 21.43% and an area of 270.68km$^2$, the low forest had 27.54% with an area of 347.8km$^2$ and the waterbody had 6.30% with an area of 79.62km$^2$.

The distribution of class within the high-risk flood zone is shown in Table 19 and Figure 21.

**Table 19. Distribution of feature class at risk of high-risk flooding**

| S/N | Class Name | Area | Percentage |
|---|---|---|---|
| 1 | Built up area | 564.43 | 44.70 |
| 2 | High Forest | 270.68 | 21.43 |
| 3 | Low Forest | 347.8 | 27.54 |
| 4 | Waterbody | 79.62 | 6.30 |
| | Total | 1262.53 | 100.00 |

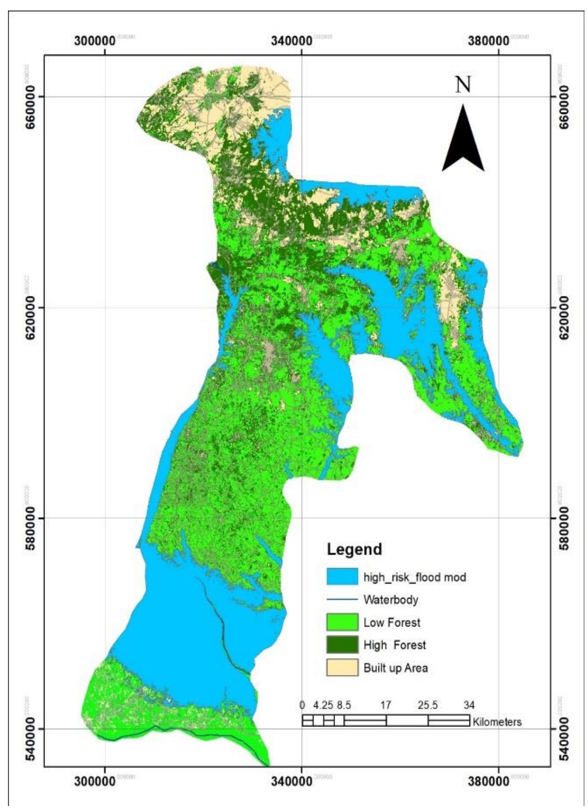


Fig. 21 High-risk zone as modeled by flood modeler

*3.7.11. Features at Moderate Risk of Flooding*

The results showed that built up area had 50.33% with an area of 749.55km$^2$ in the moderate-risk area, while the high forest had 26.19% and an area of 390.09km$^2$, the low forest had 20.02% with an area of 298.21km$^2$ and the waterbody had 4.43% with an area of 66.06 km$^2$. The distribution of class within the moderate risk flood zone is shown in Table 20 and Figure 4.22.

**Table 20. Distribution of feature class at moderate risk**

| S/N | Class Name | Area | Percentage |
|---|---|---|---|
| 1 | Built Up Area | 749.55 | 50.33 |
| 2 | High Forest | 390.09 | 26.19 |
| 3 | Low Forest | 298.21 | 20.02 |
| 4 | Waterbody | 66.06 | 4.43 |
| | Total | 1489.25 | 100 |

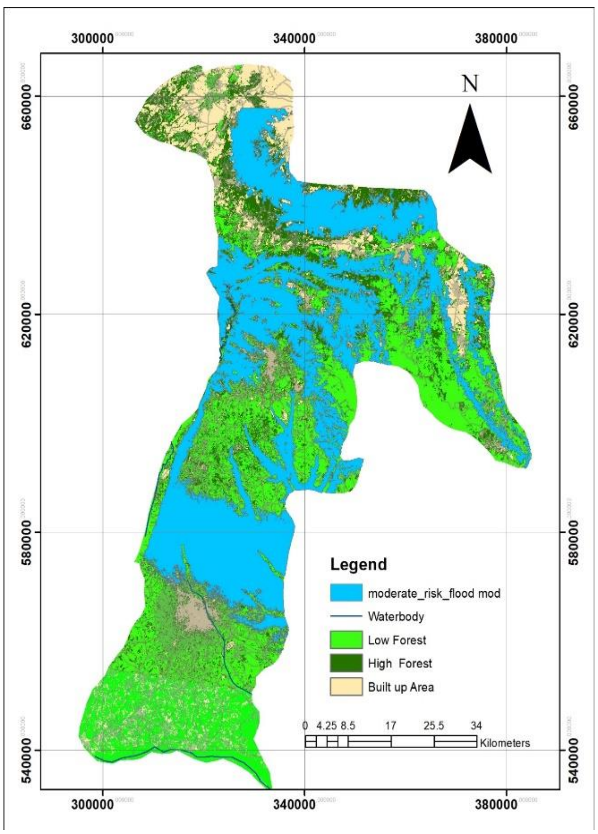


**Fig. 22 Moderate-risk zone as modeled by flood modeler**

*3.7.12. Features at Low Risk Flooding*

The results showed that built up area had 45.32% with an area of 606.77km$^2$ in the low-risk area, while the high forest had 27.88% and an area of 373.29km$^2$, the low forest had 24.77% with an area of 331.69km$^2$ and the waterbody had 2.23% with an area of 29.96 km$^2$. The distribution of class within the moderate risk flood zone is shown in Table 21 and Figure 4.23.

**Table 21. Distribution of feature class at low risk flooding**

| S/N | Class Name | Area | PERCENTAGE |
|---|---|---|---|
| 1 | Built up area | 606.77 | 45.32 |
| 2 | High Forest | 373.29 | 27.88 |
| 3 | Low Forest | 331.69 | 24.77 |
| 4 | Waterbody | 26.96 | 2.23 |
| | TOTAL | 1338.71 | 100 |

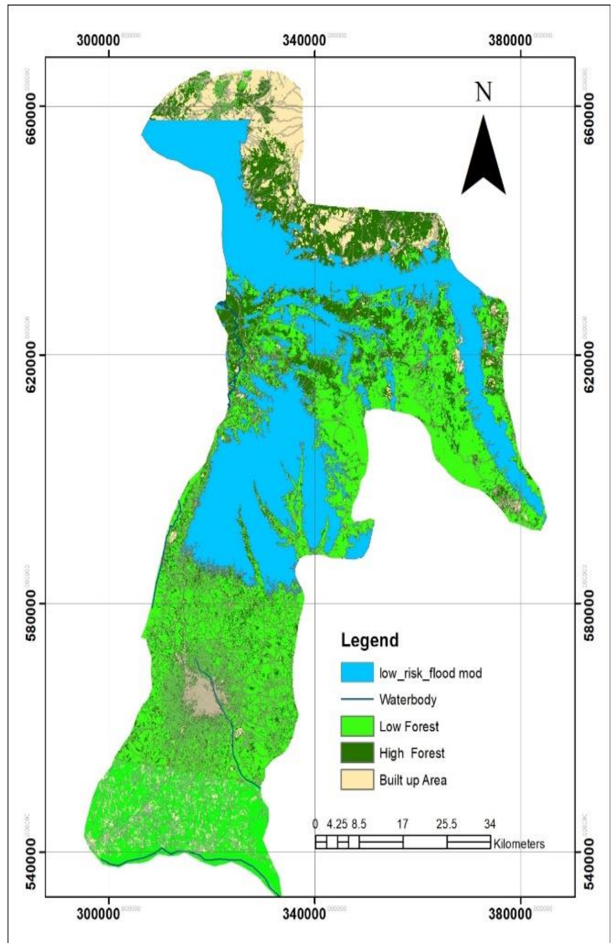


**Fig. 23 Low-risk zone as modeled by flood modeler**

***3.8. Validation of HEC-RAS, TUFLOW and Flood Modeler Results***

In order to determine the best fit model for flood modelling in the study area, ground validation is needed to determine the reliability and accuracy of the flood modeling results of HEC-RAS, TUFLOW and Flood modeler.

The modelled zone points were compared to flood points obtained from the ground. These sample points were coded and compared using the correlation coefficient. The results are illustrated in Figures 24, 25 and 26.

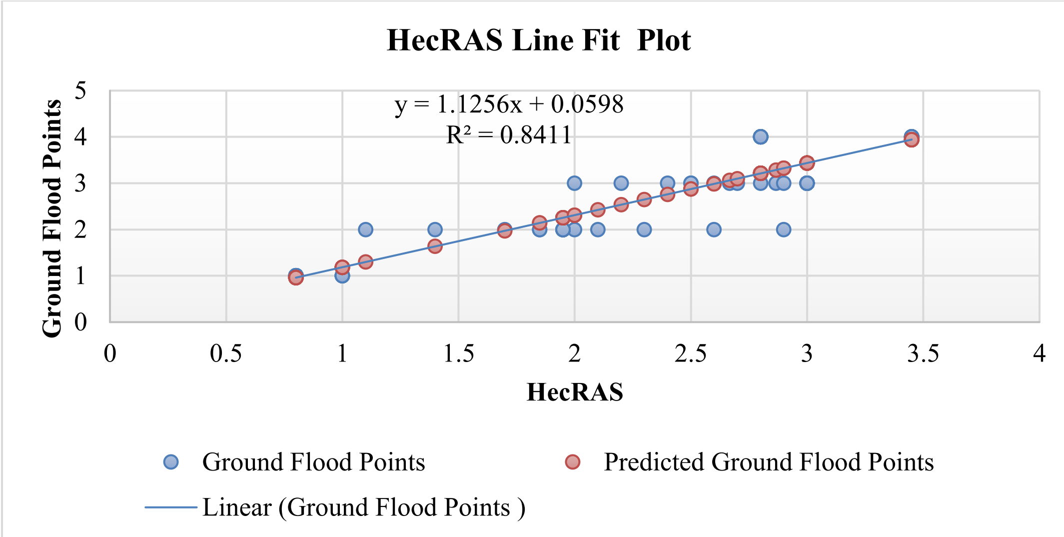


**Fig. 24 Line fit plot of HEC-RAS modelled result against ground flood points**

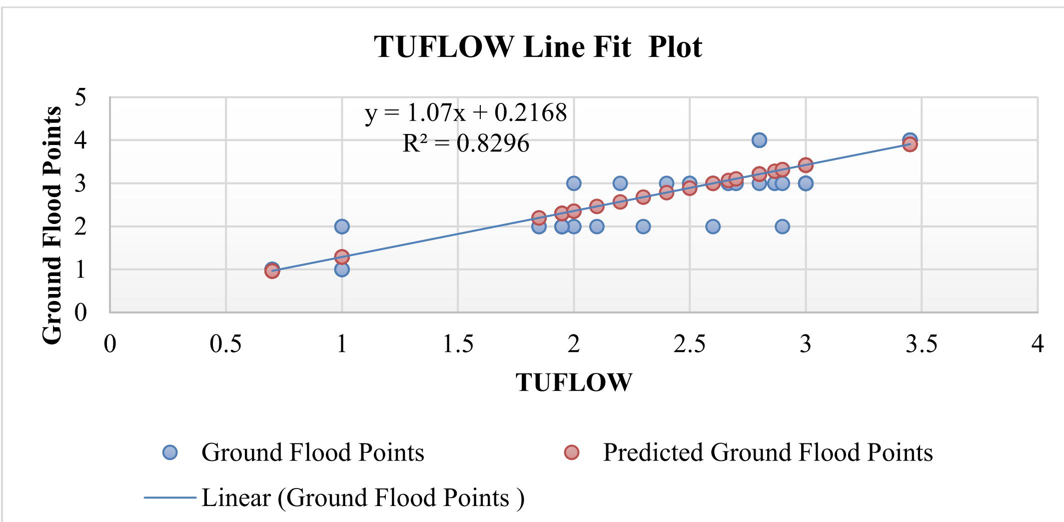


**Fig. 25 Line fit plot of TUFLOW modelled result against ground flood points**

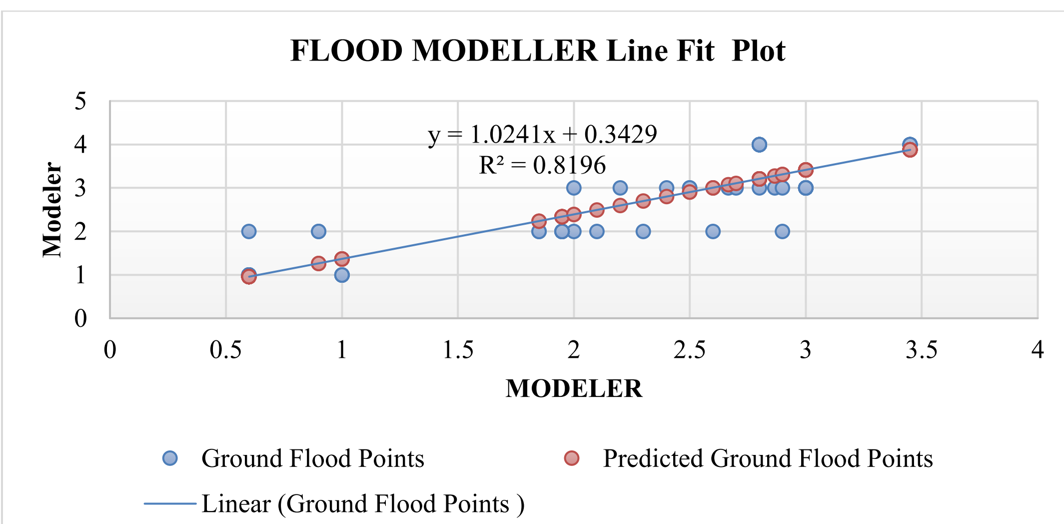


**Fig. 26 Line fit plot of the Flood modeler modelled result against ground flood points**

The results of the correlation analysis revealed that HEC-RAS modelled result (figure 24) obtained a coefficient of 0.8411 and standard error of 0.44 against the ground flood points, TUFLOW modelled result (25) obtained a coefficient of 0.8296 and standard error of 0.46 against the ground flood points while flood modeler modelled result (26) obtained a coefficient of 0.8196 and standard error of 0.48 against the ground flood points. These results indicated that out of the three models tested, HEC-RAS came out on top as having the best fit to the ground flood points, followed by TUFLOW and Flood modeler in last place.

## 4. Conclusion

Flood modelling is a crucial tool in developing policies for flood risk management. As discussed extensively, flooding remains a frequent disaster that must be tackled with accurate modern floodplain modelling and management. It is therefore pertinent to ensure that the software procedure used must produce reliable results. Out of the three models tested, HecRAS came out on top as having the best fit to the ground flood points, followed by TUFLOW and Flood modeler in last place. HEC-RAS is also recommended for use in predicting flood frequency returns, as this provides information on the future extent of flood frequency. This will enable the adequate planning and management of flooding in Abia State.

## Data Availablity

The reference cited as T.E. Ologunorisa and A. Akinbobola, Assessment of Social Vulnerability to Flood Risk in the Niger Delta, Nigeria, in Regional Climate Change Series: Floods, WASCAL Publishing, 2019, pp. 68-73, doi:10.33183/2019.rccs.p68, is recognized as a legitimate scholarly publication. However, the publication is not available through online sources. In accordance with the journal's reference policy requiring online accessibility of cited sources, this reference is acknowledged as an offline publication. Its inclusion is intended to recognize its academic significance, and its offline availability is hereby confirmed through this Data Availability Statement.

## Conflicts of Interest

There is no conflict of interest in this work.


## Funding Statement

Research has no funding from any sources.


## References


[1] Iguniwari Thomas Ekeu-Wei, George Alan Blackburn, and Jason Giovannettone, "Accounting for the Effects of Climate Variability in Regional Flood Frequency Estimates in Western Nigeria," *Journal of Water Resource and Protection*, vol. 12, no. 8, pp. 690-713, 2020. [CrossRef] [Google Scholar] [Publisher Link]

[2] Nura Umar, and Alison Gray, "Flooding in Nigeria: A Review of its Occurrence and Impacts and Approaches to Modelling Flood Data," *International Journal of Environmental Studies*, vol. 80, no. 3, pp. 540-561, 2023. [CrossRef] [Google Scholar] [Publisher Link]

[3] Adaku Jane Echendu, "Flooding and Waste Disposal Practices of Urban Residents in Nigeria," *GeoHazards*, vol. 4, no. 4, pp. 350-366, 2023. [CrossRef] [Google Scholar] [Publisher Link]

[4] Desmond R. Eteh et al., "Assessing the Impact of Climate Change on Flood Patterns in Downstream Nigeria using Machine Learning and Geospatial Techniques (2018-2024)," *Discover Geoscience*, vol. 3, no. 1, 2025. [CrossRef] [Google Scholar] [Publisher Link]

[5] T.E. Ologunorisa, and A. Akinbobola, "Assessment of Social Vulnerability to Flood Risk in the Niger Delta, Nigeria," *Regional Climate Change Series: Floods*, pp. 68-73, 2019.

[6] Eteh Desmond Rowland, and Okechukwu Okpobiri, "Floodplain Mapping and Risks Assessment of the Orashi River using Remote Sensing and GIS in the Niger Delta Region, Nigeria," *Journal of Geographical Research*, vol. 4, no. 2, pp. 10-16, 2021. [CrossRef] [Google Scholar] [Publisher Link]

[7] Kofo A. Aderogba, "Substantive Causes and Effects of Floods in South Western Nigeria and Sustainable Development of the Cities and Towns," *Journal of Emerging Trends in Educational Research and Policy Studies*, vol. 3, no. 4, pp. 551-560, 2012. [Google Scholar] [Publisher Link]

[8] Binh Pham-Duc, Catherine Prigent, and Filipe Aires, "Surface Water Monitoring within Cambodia and the Vietnamese Mekong Delta over a Year, with Sentinel-1 SAR Observations," *Water*, vol. 9, no. 6, pp. 1-21, 2017. [CrossRef] [Google Scholar] [Publisher Link]

[9] Becky P. Bamiekumo et al., "Machine Learning-based Flood Extent Mapping and Damage Assessment in Yenagoa, Bayelsa State, using Sentinel-1 and 2 Imagery (2018-2022)," *Discovery Nature*, vol. 2, no. 3, pp. 1-17, 2025. [CrossRef] [Google Scholar] [Publisher Link]

[10] Ebiegberi Oborie, and Eteh Desmond Rowland, "Flood Influence using GIS and Remote Sensing based Morphometric Parameters: A Case Study in Niger Delta Region," *Journal of Asian Scientific Research*, vol. 13, no. 1, pp. 1-15, 2023. [CrossRef] [Google Scholar] [Publisher Link]

[11] Okechukwu Okpobiri et al., "Using Machine Learning and GIS to Monitor Sandbars along the River Niger in the Niger Delta, Nigeria," *International Journal of Environmental and Climate Change*, vol. 15, no. 2, pp. 182-203, 2025. [CrossRef] [Google Scholar] [Publisher Link]